Multiplexed PCR to measure *in situ* growth rates of uropathogenic *E. coli* during experimental urinary tract infection.

Santosh Paudel[1], Geoffrey B. Severin[1], Ali Pirani[1], Melanie M. Pearson[1], Mark T. Anderson[1], Evan S. Snitkin[1,2], Harry L.T. Mobley[1*]
[1]Department of Microbiology and Immunology, and
[2]Department of Internal Medicine, University of Michigan Medical School, Ann Arbor, USA

*corresponding author

Abstract

Measuring bacterial growth rates *in vitro* is routine, however, determining growth rates during infection within a host has been more challenging. Peak-to-trough ratio (PTR) is a technique for studying microbial growth dynamics, calculated using the ratio of replication origin (*ori*) copies to those of the terminus (*ter*), as originally defined by whole genome sequencing (WGS). WGS presents significant challenges in terms of expense and data analysis complexity due to the presence of host DNA in the samples. Here, we used multiplexed PCR with fluorescent probes to estimate bacterial growth rates based on the abundance of *ori*- and *ter*-adjacent loci, without the need for WGS. We establish the utility of this approach by comparing growth rates of the uropathogenic *Escherichia coli* (UPEC) strain HM86 by WGS (PTR) and qPCR to measure the equivalent *ori:ter* ($O:T^{PCR}$). We found that PTR and $O:T^{PCR}$ were highly correlated and that $O:T^{PCR}$ reliably predicted growth rates calculated by conventional methods. $O:T^{PCR}$ was then used to calculate the *in situ E. coli* growth rates in urine, bladder, and kidneys collected over the course of a week from a murine model of urinary tract infection (UTI). These analyses revealed that growth rate of UPEC strains gradually increased during the early stages of infection (0–6h), followed by a slow decrease in growth rates during later time points (1-7 days). This rapid and convenient method provides valuable insights into bacterial growth dynamics during infection and can be applied to other bacterial species in both animal models and clinical infections.

Importance

Accurately measuring bacterial growth rates in the host, which plays a crucial role in determining the success of pathogens in establishing infections, poses significant challenges. To address this, bacterial replication rate has been measured as a proxy for growth rate estimation. While whole genome sequencing (WGS) has been used for this purpose, it comes with drawbacks such as high costs and difficulties in analyzing bacterial sequences due to the overwhelming presence of host DNA. In this study, we validate a more accessible PCR-based approach compared to the established WGS method and confirmed the reliability of our PCR-based technique. We then applied it to measure the growth rate of *Escherichia coli* during experimental urinary tract infection in a mouse model. This study provides a cost-effective and efficient alternative to WGS for studying bacterial replication dynamics during infection, potentially offering new insights into pathogen behavior and host-microbe interactions.

Introduction

Urinary tract infections (UTIs) are among the most prevalent bacterial infections, with *Escherichia coli* being the primary causative agent constituting approximately 75% of uncomplicated UTIs and 65% of complicated UTI cases (1). While the virulence factors and pathogenicity of uropathogenic *E. coli* (UPEC) are generally appreciated (1–3), the *in vivo* growth dynamics during UTIs remain less well understood. Bacterial replication rate is important to pathogenicity as it can influence evasion of the host response, colonization, and persistence (4). Understanding bacterial growth rates within different infection niches will also advance our knowledge of how each unique environment affects bacterial proliferation and the progression of infection and helps pinpoint specific factors responsible for promoting or inhibiting bacterial growth.

Recent studies have established the use of bacterial circular chromosome replication as a means to determine growth rates with the underlying principle that rapidly growing bacteria have multiple replication forks starting at the origin (*ori*), leading to greater abundance of DNA proximal to the *ori* than distal sequences located near the terminus (*ter*) whereas slow growing or stationary phase bacteria have a more equitable number of *ori* and *ter* loci (Fig. 1). The ratio of sequencing coverage between the *ori* and *ter*, obtained from whole genome sequencing (WGS), is referred to as the peak-to-trough ratio (PTR) and was first applied by Korem *et al*. in 2015 for the determination of bacterial growth rates in a metagenomic study (5). Subsequently, a number of studies have utilized the concept of PTR to measure bacterial growth rates under a variety of conditions using WGS (5–12), digital droplet PCR (13), and SYBR green dye-based quantitative real time PCR (qPCR) (14, 15). While WGS-based PTR has been widely applied and allows for the quantification of both *ori* and *ter* adjacent sequence abundance within the same sample, this method is expensive, requires computational resources and expertise, and generates an unnecessary amount of sequencing data if growth rate determinations are the sole objective. While techniques utilizing qPCR-based methods offer a more economical approach to specifically quantify *ori* and *ter* adjacent sequences, their reliance non-specific DNA-intercalating dyes necessitates that the quantification of *ori* and *ter* abundance in the same sample be measured independently from one another. In our study, we combine both the ease of in-house qPCR with the WGS benefit of simultaneous measurement of *ori* and *ter* abundance in the same sample reaction by multiplexing qPCR reactions using TaqMan probes, and designate this $O{:}T^{PCR}$.

The purpose of this study was two-fold: 1) to develop a probe-based multiplexed qPCR method for measuring *ori:ter* and 2) to use this method to determine the growth rates of UPEC strains *in vivo* during experimental urinary tract infection in mice. Validation of this approach streamlines the process of determining *ori:ter* to accurately and rapidly estimates doubling times in diverse biological samples. Measuring bacterial growth rate *in vivo* within host tissue may provide insight into the dynamics of experimental infections over time and the possibly clinical outcomes. After validating our qPCR

method with conventional PTR measured by WGS, we determined the growth dynamics of two UPEC strains HM56, and HM86 *in vivo* during experimental murine UTI for 7 days post inoculation. We found both UPEC strains rapidly replicating in murine urine sample early in the infection (6–12 hpi) with growth rates slowly decreasing through the course of a week. This study demonstrates the usefulness of applying a probe-based qPCR method to measure UPEC growth rates in a clinically relevant model of UTI, which could be leveraged for use in various types of infections and models.

Materials and methods

Bacterial strains and culture conditions

E. coli strains HM56 and HM86 were isolated from cases of uncomplicated UTI and have been described elsewhere (16, 17). Bacterial strains were revived from the frozen stock (-80°C) by culturing overnight in Lysogeny broth (LB), aerating at 200 rpm at 37°C. To conduct an *in vitro* experiment, the HM86 strain was cultured overnight with aeration at 37°C in LB, and inoculated 1:100 in fresh LB, terrific broth (TB), M9 minimal growth medium supplemented with 0.4% glucose ($M9_{Glc}$), and pooled human urine (HU) from healthy female volunteers. We sampled bacteria from the culture at 0, 1, 1.5, 2, 2.5, 3, 3.5, 4, 5, and 6h to assess bacterial growth rate in different growth media, measuring absorbance (OD_{600}) in cuvettes using GENESYS 10S VIS spectrophotometer (Thermo Scientific). We collected bacterial pellets for each time point by centrifugation at 17K x *g* (Fisher Accuspin Micro 17R) for genomic DNA. The bacterial pellet was immediately placed in dry ice and stored at -80°C until further processing. Bacterial growth rate was determined using the formula:

Growth rate (GR_p) = ($\log(OD_{p+t}/OD_{p-t})$)/dt, where “p” is the time point whose $O{:}T^{PCR}$ values is correlated with the growth rate, “p-t” is the initial OD, “p+t” is the final OD, “dt” is the time elapsed between initial and final OD. For our growth rate calculation, t=30 minutes. Bacterial doubling time (DT) *in vitro* was calculated as [$\log(2)/GR_p$].

Quantitative polymerase chain reaction (qPCR)

Genomic DNA (DNA) from *in vitro* bacterial culture samples and mice urine and organs were extracted using DNeasy® Blood and Tissue Kit (Qiagen, Germany) following manufacturer’s instruction. The qPCR was performed to determine the *ori:ter* ratio, a proxy of PTR (referred in this study as $O{:}T^{PCR}$). The DNA concentration was estimated using Nanodrop One (Thermo scientific). The bacterial DNA in concentration of 500 pg was used to determine PTR for the *in vitro* samples. The targeted nucleotide sequences for the qPCR reaction near the origin of the replication (*ori*) is the *gidA* gene, and near the terminus of replication (*ter*) is the *dcp* gene.

The qPCR reaction was performed in QuantStudio 3 (Applied Biosystems) thermocycler (95°C 30 s, 40×(95 °C 5 s+58 °C 30 s). The optimized 25 µl reaction mixture contained 12.5 µl TaqMan™ Fast Advanced Master Mix (Applied biosystems), 2.5 µl template DNA, and 10 µl of the reaction mixture of forward and reverse primer for *ori* and *ter*

region (final primer concentration 1μM each), and probe for *ori* and *ter* sequence (concentration 0.25μM each). The annealing efficiency of the primer and probe binding to the *ori* and *ter* oligos was calculated using the equation [(E)= 10^(-1/slope)-1] where E represents the annealing efficiency, and slope is derived from the standard curve of 10-fold dilution of DNA (5000 to 0.5 pg). To ensure the reliability and accuracy of the qPCR results, we repeated certain samples using a second set of primers that targeted the same region with the same probes for both set of primers. Primers (14, 18) and probes used for qPCR are provided in Table 1. The $O:T^{PCR}$ was determined using $2^{-\Delta\Delta Ct}$ method ($\Delta Ct = Ct_{ori} - Ct_{ter}$; $\Delta\Delta Ct = \Delta Ct_{test} - \Delta Ct_{reference}$). The PTR for each sample is the average PTR of 3 technical replicates. The sample of the same bacterial strain cultured to stationary phase of growth, whose peak-to-trough is expected to be 1, is used for the normalization during each run. To evaluate the specificity of the primers and probes utilized in the experiment we performed two experiments: 1) using DNA from various Gram-positive and Gram-negative bacteria, both individually and mixed with *E. coli* DNA (1:1) to determine whether the presence of DNA from other bacterial sources affect the *ori:ter* ratio, and 2) inclusion of DNA extracted from murine kidney to assess the *E. coli* DNA-specificity of the qPCR in the presence of mouse genetic material. Molecular biology grade water (Corning) was used as non-template control (NTC) for each cycling run. The sample tested for PTR using WGS was incorporated in every set of the qPCR performed to minimize the experimental variability in PTR measurements between experiments. The qPCR assay was performed for the UPEC strains cultured *in vitro* in LB, TB, $M9_{Glc}$ and *in vivo* samples from the mouse during UTI.

Whole genome sequencing

PTR values were determined using previously published methods (5, 6). Briefly, sequenced reads from each sample were cleaned and mapped to the complete genome sequence of the originating bacterial isolate using Trimmomatic v0.39 and Bowtie2 v2.5.1. All alignments were indexed and sorted using SAMtools v1.18, and the coverage depth for each nucleotide position was extracted using Bedtools v2.30.0. A smoothing filter was applied to the mapped coverage of genomic segments, which was comprised of a moving sum with a window size of 10 kbp and a slide of 100 bp, followed by a moving median with a window size of 10-kbp bins and a slide of 100 bins. Instances where the bins did not have any mapped reads or had <50% remaining bins were discarded. The PTR was calculated from the peak and trough read coverage locations corresponding to maximum and minimum values, respectively, from the smoothed coverage (5). Snakemake implementation and analysis results can be accessed at https://github.com/alipirani88/Growth-rate-estimate_SMAKE. Assemblies for HM86 and HM68 were generated with Flye 2.9.2 and annotated with Prokka 1.14.5. Origin and termination of replication sites were determined by blasting qPCR OriC and Ter loci using BLAST 2.14.0

164 **Mouse model of ascending UTI**

165 Six-to-eight weeks old female CBAJ (Jackson laboratory) mice were inoculated
166 transurethrally with ~$2x10^8$ CFUs of UPEC strains as described previously (19, 20).
167 Briefly, the overnight culture of UPEC strains cultured with shaking at 37°C was
168 centrifuged for 30 minutes at 3000 rpm and the bacterial pellet was resuspended in
169 sterile PBS. Mice were anaesthetized using ketamine/xylazine intraperitoneally (IP).
170 Then, 50 µl of bacterial suspension was inoculated transurethrally using a sterile
171 polyethene catheter connected to an infusion pump (Harvard Apparatus). After the
172 induction of the UTI, urine samples from the inoculated mice were collected at 6, 24, 48,
173 72, 96, 120, 144, and 168 hpi for determination of CFUs and isolation of bacterial DNA.
174 Mice were euthanized at 6, 24, and 168 hpi, and bladder and kidneys were collected for
175 bacterial burden and bacterial DNA in the tissue samples. The bladder, and kidneys
176 were collected in 5 ml culture tubes with 2 ml of ice-cold sterile PBS and homogenized
177 using homogenizer (GLH 850, OMNI International). Bacterial burden from urine and
178 each organ was enumerated using dilution plating by the drip-plate method and
179 incubation at 37˚C. The limit of detection (LOD) of bacteria in urine was 10^3 CFU/ml,
180 whereas for bladder and kidney is 20 CFU/organ. Urine and tissue homogenates were
181 centrifuged at 17K x *g* at 4°C for 5 minutes. The supernatant was discarded, and the
182 pellet was placed immediately on dry ice and stored at -80°C until further processing for
183 DNA to measure bacterial growth rate determining PTR.

184 **Statistical analysis**

185 Correlations between PTR and $O:T^{PCR}$, and bacterial growth rate and $O:T^{PCR}$ were
186 evaluated using Pearson's correlation coefficient. Linear regression analysis was
187 performed to establish the relationship between growth rate and $O:T^{PCR}$. Statistical
188 significance of the doubling time (DT) measured by OD and PTR was determined using
189 the paired *t*-test. To test the significance of *E. coli* burden in bladder, kidney, and urine
190 as well as $O:T^{PCR}$ in urine, we employed the Kruskal-Wallis test. Statistics and
191 illustrations were performed using GraphPad Prism version 10 (GraphPad Software,
192 CA, USA). A two-tailed *p*-value < .05 was considered statistically significant.

193 ## Results

194 **Validating multiplexed quantitative real time PCR with whole genome sequencing**
195 **as a tool for measuring origin to terminus ratios *in vitro***

196 To compare WGS PTR with our qPCR *ori:ter* method, we first generated a standard
197 curve relating the growth rates of bacterial populations cultured *in vitro* to the relative
198 abundance of the corresponding *ori* and *ter* sequences. This was achieved by culturing
199 the *E. coli* strain HM86 in three different media where rapid and slow bacterial growth
200 could be observed: lysogeny broth (LB), terrific broth (TB) and an M9 minimal medium
201 containing glucose ($M9_{Glc}$). Growth curves were initiated by addition of a one-to-one-
202 hundred dilution of stationary phase HM86 culture into fresh medium and the optical
203 density (OD_{600}) of the bacterial population was measured at 30 to 60 minutes intervals

204 over the six-hour period. Concurrent with these OD_{600} measurements, cell pellets were
205 collected for genomic DNA extraction from which the relative abundance of the *ori* and
206 *ter* sequences in the bulk population were measured by both multiplexed qPCR and
207 WGS.

208 As anticipated, *E. coli* HM86 grew rapidly in both rich media (LB and TB) (Fig. 2 A)
209 achieving exponential growth as early as 1.5 h post-inoculation and transitioning into
210 stationary phase approximately two-hours later. In contrast, growth in $M9_{Glc}$ was
211 markedly slower with a longer lag phase and achieving a greatly reduced bacterial
212 density over the course of six hours (Fig. 2A).

213 We first performed WGS on DNA samples collected throughout these growth curves to
214 measure the relative abundance of *ori* and *ter* regions. Figure 2B illustrates one such
215 read coverage plot from *E. coli* HM86 cultured in LB medium (Fig. 2A). During periods
216 of rapid population expansion (1 – 3 h), we observed higher sequencing coverage (*i.e.*,
217 peak) around the *ori* and lower sequencing coverage (*i.e.*, trough) corresponding with
218 the location of the *ter*. As expansion of the population slowed, the relative abundance of
219 reads mapping to the *ori* and *ter* regions normalized, resulting in a PTR of ~1. Plotting
220 the PTR from WGS data across the rich media growth conditions (Fig. 2C) illustrates
221 the dynamic transition in PTR throughout the course of the growth curves (LB and TB, n
222 = 3) with mean maximal PTR being observed at 1.5 h (LB = 1.68 ± 0.14, TB = 1.73 ±
223 0.1). While WGS was only performed for a single population of *E. coli* HM86 cultured in
224 low nutrient $M9_{Glc}$, the very modest changes in PTR predictably corresponded to the
225 slow increase in culture density over time with a maximal PTR of 1.28 at 6 h (Fig. 2A).

226 We next tested whether multiplexing qPCR was a viable alternative to WGS for
227 measuring the relative abundance of *ori* and *ter* sequences using these same *in vitro*
228 DNA samples. Using previously published primers (14) and newly designed probes
229 specific for regions near the *ori* and *ter,* we were able to rapidly generate *ori:ter* ($O:T^{PCR}$)
230 for *E. coli* HM86 cultured in all three media (Fig. 2D). Similar to PTR (Fig. 2B), the
231 relative *ori:ter* measured by $O:T^{PCR}$ in rich media were greatest during times of rapid
232 population expansion with mean maximal *ori:ter* measured at 1.5 h (LB = 2.56 ± 0.12,
233 TB = 2.69 ± 0.28) and this ratio gradually normalized to ~1 as cultures reached
234 stationary phase (Fig. 2A). We also observed that the *ori:ter* in $M9_{Glc}$ also demonstrated
235 a modest change in the $O:T^{PCR}$ reflective of the slow and limited expansion of the *in vitro*
236 population over time (Fig. 2A) with a mean maximal *ori:ter* of 1.43 ± 0.05 measured at
237 3.5 h. While the relationship between the *ori:ter* and *in vitro* culture growth phases were
238 similar between PTR and $O:T^{PCR}$ in all three media, the maximal values of the *ori:ter*
239 during times of population expansion were greater when measured by multiplexed
240 qPCR than WGS (Figs. 2C & 2D). Despite differences in the absolute values of $O:T^{PCR}$
241 and PTR, we found the measurements *ori:ter* and PTR of each individual DNA sample
242 were highly correlated in all three media conditions (Figs. 2E, 2F & 2G). We also
243 performed the growth experiment of *E. coli* strain HM86 in human urine for 6h and
244 measured PTR and $O:T^{PCR}$ and found near perfect correlation of the measurements

245 derived from WGS and qPCR methods (r=0.99, p=0.0002) (Fig. S3). The data revealed
246 the slow growth of *E. coli* in vitro in human urine. The difference in absolute magnitude
247 of *ori:ter* is likely reflective of a greater dynamic range in measuring *ori* and *ter*
248 abundance by multiplexed qPCR and correlation of these measurements with PTR
249 demonstrates the viability of using probe-based qPCR in lieu of WGS.

250 **O:T^{PCR} accurately predicts bacterial growth rate *in vitro***

251 Having demonstrated O:T^{PCR} is a reliable method to measure *ori:ter*, we then calculated
252 growth rates for each time point across every growth curve based on the OD_{600}
253 measurements that immediately preceded and followed that time point. A standard
254 curve of growth rate and O:T^{PCR} was then established from all time points where the
255 median growth rate from biological replicates cultured in same medium was less than
256 0.0025 (*i.e.*, doubling time of 120 min) (Fig. 3A). This minimum doubling time criterion
257 functionally incorporated all regions of the three growth curves where active growth
258 could be observed (*i.e.*, excluded lag and stationary phases) and the O:T^{PCR} were in
259 excess of 1.25 and these time points are illustrated as filled symbols in Fig. 1A and 1D.
260 From these data, we could construct a standard curve and derive a linear equation
261 (Y=0.007648*X-0.006786) based on the relationship between growth rate and O:T^{PCR}
262 (Fig. 3A). We then used this equation to calculate a predicted growth rate for all O:T^{PCR}
263 measurements included in the standard curve and found no significant difference
264 between the predicted growth rate and the experimentally derived growth from OD_{600}
265 measurements for each O:T^{PCR} measurement (Fig. 3B). The constraints of this standard
266 curve are the maximum and minimum O:T^{PCR} measurements of 2.87 and 1.16
267 representing a doubling times of 19.9 and 143.0 minutes, respectively. Therefore,
268 O:T^{PCR} which are greater or less than these extremes cannot be used to accurately
269 determine bacterial growth rates and are instead defined as extremely rapid growth or
270 slow growth, respectively.

271 **Establishing limits of *ori:ter* quantification, detection, and specificity of O:T^{PCR}**

272 Under optimal conditions, such as bacterial monoculture, bacterial DNA can be
273 extracted, quantified, and used in downstream molecular applications with the
274 knowledge that all the nucleic acids present originated from a single source. In an
275 infection model, DNA extracted from a complex biological sample will be a mixture of
276 both host and etiological agent derived nucleic acids. Additionally, the concentration of
277 bacterial DNA within this sample will be unknown and likely to be in low abundance.
278 Therefore, we established two constraints for accurate *ori:ter* determination by O:T^{PCR} in
279 complex biological samples: a limit of quantification (LOQ) establishing the minimum
280 number of CFU (LOQ-CFU) from which DNA could be extracted and accurately
281 measured, and LOQ-DNA demonstrating the minimum quantity of bacterial DNA which
282 can be accurately measured.

283 Because the total number of CFU collected in a biological sample from an infection model
284 can vary, we chose to establish LOQ which would represent the minimum number of

285 bacterial cells required to provide adequate template DNA for accurate O:T^{PCR}
286 determination. To establish this LOQ, we cultured *E. coli* HM86 to exponential phase in
287 LB for 2 h from which 10-fold serial dilutions were prepared and DNA extractions of ~10^6,
288 10^5, 10^4, 10^3, 10^2, 10, and 0 CFUs were performed. From these DNA extractions we found
289 the relationship between *ori* and *ter* was measured to be approximately 2.23±0.09 by
290 O:T^{PCR} from templates originating from extractions containing 10^6 to 10^3 CFU, while those
291 extracted from fewer CFU resulted in a significant deviation in this ratio (Fig. 4A).
292 Therefore, an LOQ of ≥ 10^3 CFU is required to provide sufficient bacterial DNA template
293 for accurate determination of *ori:ter* by O:T^{PCR} .

294 In a biological sample collected from the infection model, bulk DNA extraction is likely to
295 capture DNA from both the infectious agent and the host. This complex mixture of nucleic
296 acids is likely to obscure the direct quantification of input template prior to its application
297 in O:T^{PCR} . Because template abundance is correlated with critical threshold (Ct) values
298 obtained by qPCR, we sought to define an LOQ based on the greatest Ct value for the
299 *ori* specific oligo primers from which the relationship of *ori:ter* can be reliably determined
300 by O:T^{PCR} . Using DNA extracted from ~10^8 CFUs, described in the LOQ experiment
301 above, we performed O:T^{PCR} with 10-fold serial dilutions of template DNA (5 ng to 0.05
302 pg) to determine the range from which the *ori:ter* could be reliably measured. O:T^{PCR}
303 containing 5 ng to 0.5 pg template DNA consistently measured an *ori:ter* of approximately
304 2.32±0.06, and this ratio deviated as the template abundance fell below this range (Fig.
305 4B). Over the entire range of templates tested, the *ori* oligo Ct values reliably increased
306 by a mean Ct of 3.41 per 10-fold dilution of template (ideal change is 3.32 Ct per 10-fold
307 dilution). The annealing efficiency of the primers and probes for *ori* and *ter* oligos were
308 determined to be 96.2%, and 96.9 % respectively. Based on the these observations, we
309 found the highest Ct value (*i.e.*, lowest template abundance) from which *ori:ter* could be
310 determined by O:T^{PCR} was 30.52±0.97 cycles. This LOQ establishes a critical threshold
311 for informing the appropriate conditions for the application of *ori:ter* measured by O:T^{PCR}
312 ; where the *ori* oligo Ct≤30.52, the corresponding *ori:ter* can be confidently used to
313 accurately calculate the growth rate of the bacteria in that sample.

314 As described above, biological samples collected from an infection model are likely to
315 contain at least two sources of DNA; the infectious agent and the host. There also exists
316 the possibility that samples can contain DNA extracted from other sources (*e.g.*, host
317 commensals). To test the specificity of the *ori* and *ter* oligos to discriminate between *E.*
318 *coli* and from other sources of DNA we performed O:T^{PCR} on mixed DNA templates
319 containing 5 ng of *E. coli* HM86 DNA combined with of 5 ng of DNA isolated from
320 alternative sources. In the absence of extraneous DNA, the template composed of
321 exclusively *E. coli* HM86 DNA had a 16.04±0.13 *ori* oligo Ct and a 2.40±0.03 O:T^{PCR} .
322 Addition of equal amount of DNA template purified from seven Gram-negative species
323 cultured overnight (*Acinetobacter baumannii*, *Citrobacter freundii*, *Enterobacter*
324 *hormaechei*, *Klebsiella pneumoniae*, *Morganella morganii*, *Pseudomonas aeruginosa*,
325 *Serratia marcescens*), two Gram-positive species (*Bacillus subtilis* and *Staphylococcus*
326 *aureus*) (Table 2), or host murine DNA (CBAJ) (Fig. 4B) did not significantly affect the

327 detection of the *E. coli* HM86 template. While some reactivity with the *ori* and *ter* oligos
328 was observed in the absence of *E. coli* HM86 DNA template for some of these alternative
329 DNA samples, as well as the matrix control from the purification kit, the observed *ori* oligo
330 Ct values were greater than the established LOQ above (≤30.5 Ct) (Table 2) and would
331 therefore be excluded from further analysis.

332 From these standardization and specificity experiments (Fig. 4), we found that *ori* and *ter*
333 oligos are specific for *E. coli* HM86, extraction of >10^3 bacterial CFUs is needed to provide
334 enough template for $O:T^{PCR}$, and a Ct≤30.5 for the *ori* oligos is required to accurately
335 quantify the *ori:ter* in a given sample. By applying these criteria as quality control
336 measures for evaluating bacterial growth rates we can apply $O:T^{PCR}$ to complex biological
337 samples collected from an infection model.

338 To ensure the reliability of our PCR method in measuring *ori:ter* ratios, we validated the
339 same primer oligos with the other *E. coli* strain, HM56. We cultured strain HM56 in LB
340 medium for 6h and measured $O:T^{PCR}$ and found similar results to HM86, where HM56
341 DNA behaves like HM86 DNA indicating that our qPCR method is robust and applicable
342 across different *E. coli* strains (Fig. S1).

343 **Mouse model of ascending UTI**

344 Following parameterization of $O:T^{PCR}$, we applied this method to measure *in vivo* bacterial
345 growth rates in our model of interest, the experimental murine model of ascending UTI,
346 over a period of seven days. For this, we induced experimental UTI in 6–7 week CBAJ
347 female mice by transurethral catheterization and mono-culture inoculation of UPEC
348 strains HM86 or HM56 isolated from uncomplicated female UTI patients (17, 21). Urine
349 samples from the infected mice were collected at 6, 24, 48, 72, 96, 120, 144, and 168 hpi,
350 whereas bladder and kidney samples were collected at 6, 24, and 168 hpi in a separate
351 group of mice for bacterial burden and for extracting DNA and measuring growth rates
352 from the two UPEC strains (Fig. 5).

353 Urine bacterial burden showed distinct patterns of colonization for each strain in the
354 bladder, kidney and urine but no statistical significance difference in the CFU burden
355 was observed over time. *E. coli* HM56 urine samples exhibited higher initial counts at
356 6hpi, with high abundance of bacterial culture later up to 7 days period. In contrast, *E.*
357 *coli* HM86 exhibited lower urine bacterial count at 6hpi, increased by 24hpi, and
358 maintained a constant level of persistence throughout the infection period (Fig. 5B).
359 Bladder colonization was similar for both strains, with higher level of colonization at
360 6hpi, which decreased by 24hpi, and remained at similar level up to 168hpi (Fig. 5C).
361 The kidney colonization differed between the two strains. High level of kidney
362 colonization was observed for *E. coli* HM56 at 6hpi, which was found to be lowered by
363 approximately 10-fold at 168hpi. Conversely, *E. coli* HM86 exhibited limited kidney
364 colonization early during the infection (6 hpi, 1 of 5 mice) which increased in abundance
365 at later time points (24 hpi 2 of 5 mice; 168 hpi 3 of 5 mice) (Fig 5D) indicating a slower
366 time to ascension. These findings highlight strain-specific variations in colonization

367 patterns during the progression of UTI, providing insights into the dynamics of bacterial
368 colonization, dissemination, and persistence in the different sites of the urinary tract.

369 **Growth rate of UPEC strains *in vivo* during UTI**

370 Bacterial growth rates for HM86 and HM56 were next measured using DNA extracted
371 from urine, bladder and kidney homogenates from infected animals. The recovery of
372 bacterial DNA from the kidney sample was challenging due to the presence of host
373 genetic material as evidenced by the observed Ct values compared to the recovered
374 number of *E. coli* CFUs. However, the recovery was less affected in bladder and urine
375 samples as observed Ct values were similar to the experiment performed with
376 comparable known CFUs *in vitro* from pure bacterial culture. The DNA was extracted
377 from urine, bladder, and kidney samples and *ori:ter* was determined. Fig. 6 illustrates
378 the *ori:ter* values determined by qPCR from the urine samples during infection over the
379 period of 168h. We observed comparable patterns of *ori:ter* between the two tested
380 strains over the infection timeline, which shows the variability in the replication rate.
381 From these *ori:ter* -values, we can predict that the growth rate of UPEC is higher at
382 6hpi, which gradually decreases over the subsequent infection period where the median
383 *ori:ter* values is around our estimated borderline of the slow and fast growth conditions.
384 No statistically significant difference was observed in *ori:ter* -values over the course of
385 time.

386 The bacterial population doubling time was calculated from the qPCR derived *ori:ter*-
387 values using the equation derived from the linear regression analysis of *E. coli* HM86 *in*
388 *vitro* growth rate with their respective *ori:ter* value (Fig. 4D). The calculated *E. coli* DT in
389 mouse urine is presented in Table 2. These DT results revealed a gradual increase in
390 the growth rate of bacteria during the early stages of infection, peaking at 6h, followed
391 by a slow decrease during later days transitioning to slower state of growth at 168hpi.
392 The fastest median DT for *E. coli* HM56 and HM86 is 47.4 and 54.2 minutes,
393 respectively, observed for both at 6 hpi. The fastest growth of *E. coli* HM56 was
394 observed at 24 hpi with a DT of 28.9 minutes, while for *E. coli* HM86, it was found to be
395 31.3 minutes at 6hpi. In case of individual mice, at 6hpi the fastest growth was
396 determined as 31.6, and 31.3 minutes for HM56, and HM86 respectively. During the
397 later time points, the UPEC strains exhibited variable growth rates. This trend suggests
398 that UPEC undergoes rapid multiplication in the urine during early stages of UTI,
399 particularly within the first 6h, followed by a gradual slowdown in growth rate. The
400 similarity in growth rate between the two strains implies a similar growth strategy among
401 different UPEC isolates during infection. Due to the presence of lower number of CFUs
402 in most of the bladder, we were only able to determine *ori:ter* in few bladder samples
403 with Ct value within the range of LOQ. For HM86, the DT in bladder was found to be
404 33.3 minutes at 6hpi (1/5 mice), which was found slower at 24hpi with DT of 61.2
405 minutes (1/5 mice). No bladder had sufficient CFUs for *ori:ter* determination at 168hpi
406 for HM86. For HM56, in contrast to HM86, we observed slower growth at 6hpi with DT
407 of 63.1 and 71.2 minutes (2/5 mice), which became even slower at 24 and 168 hpi with

408 DT of 76.8 (1/5 mice) and 81.2 (1/5 mice) minutes respectively (Fig.S2-C). In contrast to
409 the bladder, the growth rate in kidneys was found to be slower at early stage of
410 infection, i.e., 6h followed by faster growth at 24 and 168 hpi for both *E. coli* strains. For
411 HM56, the fastest growth rate was determined with DT of 76.6, 40.2, and 43.7 minutes
412 at 6, 24, and 168 hpi, respectively. Since the kidney colonization with HM86 was limited,
413 we were only able to determine the growth rate of 1 kidney samples at 6 and 168 hpi,
414 with DT of 227.9 and 51.9 minutes, respectively (Fig. S2-D). Overall, the results
415 revealed the infection-site specific differences in the *E. coli* growth rate over the course
416 of infection period.

417 Discussion

418 In this study, we developed a PCR-based method as a reliable alternative to WGS for
419 determining bacterial growth rate targeting the specific regions near the origin and
420 terminus of replication. As a proof-of-concept, the qPCR method was conducted on *in*
421 *vitro* samples of *E. coli* HM86 cultured in both minimal and rich growth media and
422 validated the *ori:ter* with results obtained from the WGS method. The validation
423 experiments were performed using bacterial DNA isolated from the cultures grown
424 under controlled laboratory conditions. This method provides an estimate of the
425 population level PTR from the samples where bacteria are at different stages in their
426 growth cycle. A series of the control experiments were conducted to validate the growth
427 rate measurements by *ori:ter* using qPCR method for bacterial replication rates in host
428 tissues. We determined that $>10^3$ bacterial CFUs in pure culture condition gives
429 accurate *ori:ter* measurements with the Ct value of *ori* oligos around 30.5, equivalent to
430 0.5 pg of the DNA used for *ori:ter* measurements. Therefore, we consider Ct values of
431 30.5 or higher to be unreliable for determining *ori:ter*. This results ensures that the
432 *ori:ter* measurements remains accurate even when dealing with low bacterial loads in
433 host tissues during infection studies. Using this validated method, we measured the *E.*
434 *coli ori:ter* during experimental UTI from urine, bladder, and kidney samples from mice.
435 DNA extraction and *ori:ter* measurement in urine and bladder samples with the bacterial
436 count above 10^3 CFUs resulted Ct value within the range of cut-off Ct value providing
437 reliable result. This might vary as the recovery of DNA varies between the extraction
438 protocol. Below this threshold, the consistency of the *ori:ter* was compromised,
439 rendering inconsistencies of the result. In terms of DNA concentration, a total DNA
440 amount of 0.5 pg was sufficient to produce a consistent *ori:ter* value, demonstrating the
441 method's high sensitivity. We were only able to measure *ori:ter* from limited bladder
442 samples since only a few bladder samples had sufficient bacterial counts to enable
443 reliable *ori:ter* measurements within reliable range of Ct values. Although the colonized
444 kidney samples had higher number of CFUs count than that required for accurate *ori:ter*
445 measurement, we were not able to measure *ori:ter* from some kidney samples as the Ct
446 values derived from the qPCR method were higher than the cut-off Ct values. This,
447 however, was not due to the interference of the mouse kidney DNA to reading for
448 bacterial DNA as evidenced by the experiment performed by adding 50 ng of the mouse
449 kidney DNA to 0.5 pg of *E. coli* DNA without deviation in the Ct values and *ori:ter*

measurements. This might be due to the inability of our DNA extraction protocol to recover enough bacterial DNA from the mouse kidney tissue homogenate.

Experiments using two sets of primers targeting the same region yielded similar results, confirming the reliability of the performed method. Since we employed a probe-based qPCR method, it was highly specific in amplifying the target sequence from the intended bacterial species. This approach allows us to amplify and measure two targeted chromosomal regions from a single sample using their specific probes, thereby reducing discrepancies in readings between wells for the replication origin and terminus regions when determining *ori:ter* measurements. This multiplexing capability is advantageous in reducing both costs and result discrepancies compared to running samples in separate wells for the two target regions.

From the *in vivo* growth rate experiment during UTI in mice, we observed active growth in the urine samples with *ori:ter* >1 in all samples. The fastest growth was observed during the early phase of infection for the tested UPEC strains which gradually slowed during later days. Previously, the growth rate *in vivo* was determined in mouse UTI as well as human patients by determining PTR, a sequencing-based method, which revealed that UPEC strains exhibit rapid growth during human UTIs, often matching or exceeding *in vitro* rates (6). Similar to this study, DT in mouse urine and bladder during experimental UTI at 6hpi was determined to be 34.9, and 36.9 minutes respectively, with much slower growth rate at 24hpi (6).To measure the growth rate *in vivo* during UTI, another study employed qPCR-based method targeting *ori* and *ter* region (22) from the urine sample of the infected human patients with UTI, where active growth with day-to-day and inter-patient variability in growth rate was observed (22). Notably, *E. coli* strains isolated from the urinary tract demonstrate significantly higher growth rates in urine compared to fecal isolates, suggesting adaptation to the urinary environment (6). The slow growth observed during the later stage of infection in the urine and bladder might be due to the multifaceted adaptive response to the challenging host environment such as activation of bacterial stress response mechanism, increased pressure from the host immune system, formation of protective biofilm, or the development of metabolically dormant persister cells. By slowing their growth, *E. coli* can manage nutrients to persist under nutrient-limited conditions, evade host immune responses, and maintain a viable population capable of resisting elimination and potentially causing recurrent infections. This strategy underscores the complex interplay between bacterial pathogens and host defenses in the context of chronic or recurring UTIs (23–29). In contrast to urine and bladder, the *E. coli* growth rate in the kidney was found to be higher during later stages of infection which highlights the niche-specific variations in growth pattern within different areas of the urinary system. The distinct growth dynamics in the kidney suggest that this organ provides a unique environment for *E. coli* proliferation as the infection progresses. From the bacterial burden and growth rate results, we did not observe the direct connection between growth rate and total number of CFUs recovered from urine, bladder, and kidneys.

The strategy of measuring *ori:ter* to study bacterial growth rate has been applied in other infection models, such as mouse peritonitis, revealing heterogeneous growth rates within bacterial populations during infection (14), and blood-stream infections (30) showing organ specific pattern of growth rate in multiple bacterial species. The method has also been tested with slower-growing pathogens like *Xylella fastidiosa*, showing promise for assessing growth status in plant and insect vector environments (31). Importantly, this approach has also been applied to predict antibiotic treatment efficacy (32).

In conclusion, our research establishes the effectiveness of a probe-based qPCR method for measuring *ori:ter* and *in situ* determinations of bacterial growth rate in a cost-effective and efficient manner. This approach of measuring bacterial growth rate by PCR has potential applications in various infection models across different bacterial species.

Acknowledgements

We would like to acknowledge the members of the Mobley lab and Bachman Lab for their insightful feedback throughout this project. This work was supported by the funding NIAID R01AI165582 (H.L.T.M.).

References

1. Flores-Mireles AL, Walker JN, Caparon M, Hultgren SJ. 2015. Urinary tract infections: epidemiology, mechanisms of infection and treatment options. Nat Rev Microbiol 13:269–284.

2. Klein RD, Hultgren SJ. 2020. Urinary tract infections: microbial pathogenesis, host–pathogen interactions and new treatment strategies. Nat Rev Microbiol 18:211–226.

3. Subashchandrabose S, Mobley HLT. 2015. Virulence and Fitness Determinants of Uropathogenic Escherichia coli. Microbiol Spectr 3:10.1128/microbiolspec.uti-0015–2012.

4. Smith H. 1990. Pathogenicity and the Microbe in vivo: The 1989 Fred Griffith Review Lecture. Microbiology 136:377–383.

5. Korem T, Zeevi D, Suez J, Weinberger A, Avnit-Sagi T, Pompan-Lotan M, Matot E, Jona G, Harmelin A, Cohen N, Sirota-Madi A, Thaiss CA, Pevsner-Fischer M, Sorek R, Xavier RJ, Elinav E, Segal E. 2015. Growth dynamics of gut microbiota in health and disease inferred from single metagenomic samples. Science 349:1101–1106.

6. Forsyth VS, Armbruster CE, Smith SN, Pirani A, Springman AC, Walters MS, Nielubowicz GR, Himpsl SD, Snitkin ES, Mobley HLT. 2018. Rapid Growth of Uropathogenic Escherichia coli during Human Urinary Tract Infection. mBio 9:10.1128/mbio.00186-18.

7. Szafrańska AK, Junker V, Steglich M, Nübel U. 2019. Rapid cell division of Staphylococcus aureus during colonization of the human nose. BMC Genom 20:229.

8. Gibson B, Wilson DJ, Feil E, Eyre-Walker A. 2018. The distribution of bacterial doubling times in the wild. Proc R Soc B 285:20180789.

9. Brown CT, Olm MR, Thomas BC, Banfield JF. 2016. Measurement of bacterial replication rates in microbial communities. Nat Biotechnol 34:1256–1263.

10. Long AM, Hou S, Ignacio-Espinoza JC, Fuhrman JA. 2020. Benchmarking microbial growth rate predictions from metagenomes. ISME J 15:183–195.

11. Joseph TA, Chlenski P, Litman A, Korem T, Pe’er I. 2022. Accurate and robust inference of microbial growth dynamics from metagenomic sequencing reveals personalized growth rates. Genome Res 32:558–568.

12. Emiola A, Oh J. 2018. High throughput in situ metagenomic measurement of bacterial replication at ultra-low sequencing coverage. Nat Commun 9:4956.

13. Schneiders S, Hechard T, Edgren T, Avican K, Fällman M, Fahlgren A, Wang H. 2021. Spatiotemporal Variations in Growth Rate and Virulence Plasmid Copy Number during Yersinia pseudotuberculosis Infection. Infect Immun 89:10.1128/iai.00710-20.

14. Haugan MS, Charbon G, Frimodt-Møller N, Løbner-Olesen A. 2018. Chromosome replication as a measure of bacterial growth rate during Escherichia coli infection in the mouse peritonitis model. Sci Rep 8:14961.

15. Beebout CJ, Robertson GL, Reinfeld BI, Blee AM, Morales GH, Brannon JR, Chazin WJ, Rathmell WK, Rathmell JC, Gama V, Hadjifrangiskou M. 2022. Uropathogenic Escherichia coli subverts mitochondrial metabolism to enable intracellular bacterial pathogenesis in urinary tract infection. Nat Microbiol 7:1348–1360.

16. Subashchandrabose S, Hazen TH, Brumbaugh AR, Himpsl SD, Smith SN, Ernst RD, Rasko DA, Mobley HLT. 2014. Host-specific induction of Escherichia coli fitness genes during human urinary tract infection. Proc Natl Acad Sci 111:18327–18332.

17. Sintsova A, Frick-Cheng AE, Smith S, Pirani A, Subashchandrabose S, Snitkin ES, Mobley H. 2019. Genetically diverse uropathogenic Escherichia coli adopt a common transcriptional program in patients with UTIs. eLife 8:e49748.

18. Riber L, Olsson JA, Jensen RB, Skovgaard O, Dasgupta S, Marinus MG, Løbner-Olesen A. 2006. Hda-mediated inactivation of the DnaA protein and dnaA gene autoregulation act in concert to ensure homeostatic maintenance of the Escherichia coli chromosome. Genes Dev 20:2121–2134.

19. Hagberg L, Hull R, Hull S, Falkow S, Freter R, Edén CS. 1983. Contribution of Adhesion to Bacterial Persistence in the Mouse Urinary Tract. Infect Immun 40:265–272.

20. Hagberg L, Engberg I, Freter R, Lam J, Olling S, Edén CS. 1983. Ascending, unobstructed urinary tract infection in mice caused by pyelonephritogenic Escherichia coli of human origin. Infect Immun 40:273–283.

21. Shea AE, Frick-Cheng AE, Smith SN, Mobley HLT. 2022. Phenotypic Assessment of Clinical Escherichia coli Isolates as an Indicator for Uropathogenic Potential. mSystems 7:e00827-22.

22. Haugan MS, Hertz FB, Charbon G, Sahin B, Løbner-Olesen A, Frimodt-Møller N. 2019. Growth Rate of Escherichia coli During Human Urinary Tract Infection: Implications for Antibiotic Effect. Antibiotics 8:92.

23. Chromek M, Slamová Z, Bergman P, Kovács L, Podracká L, Ehrén I, Hökfelt T, Gudmundsson GH, Gallo RL, Agerberth B, Brauner A. 2006. The antimicrobial peptide cathelicidin protects the urinary tract against invasive bacterial infection. Nat Med 12:636–641.

24. Nielsen KL, Dynesen P, Larsen P, Jakobsen L, Andersen PS, Frimodt-Møller N. 2014. Role of Urinary Cathelicidin LL-37 and Human β-Defensin 1 in Uncomplicated Escherichia coli Urinary Tract Infections. Infect Immun 82:1572–1578.

25. Hayes BW, Abraham SN. 2016. Innate Immune Responses to Bladder Infection. Microbiol Spectr 4:10.1128/microbiolspec.uti-0024–2016.

26. Haraoka M, Hang L, Frendéus B, Godaly G, Burdick M, Strieter R, Svanborg C. 1999. Neutrophil Recruitment and Resistance to Urinary Tract Infection. J Infect Dis 180:1220–1229.

27. Haschka D, Hoffmann A, Weiss G. 2021. Iron in immune cell function and host defense. Semin Cell Dev Biol 115:27–36.

28. Ganz T, Nemeth E. 2015. Iron homeostasis in host defence and inflammation. Nat Rev Immunol 15:500–510.

29. Nairz M, Haschka D, Demetz E, Weiss G. 2014. Iron at the interface of immunity and infection. Front Pharmacol 5:152.

30. Anderson MT, Brown AN, Pirani A, Smith SN, Photenhauer AL, Sun Y, Snitkin ES, Bachman MA, Mobley HLT. 2021. Replication Dynamics for Six Gram-Negative Bacterial Species during Bloodstream Infection. mBio 12:10.1128/mbio.01114-21.

31. Sicard A, Castillo AI, Voeltz M, Chen H, Zeilinger AR, Fuente LDL, Almeida RPP. 2020. Inference of Bacterial Pathogen Instantaneous Population Growth Dynamics. Mol Plant-Microbe Interact 33:402–411.

32. Haugan MS, Løbner-Olesen A, Frimodt-Møller N. 2018. Comparative Activity of Ceftriaxone, Ciprofloxacin, and Gentamicin as a Function of Bacterial Growth Rate Probed by Escherichia coli Chromosome Replication in the Mouse Peritonitis Model. Antimicrob Agents Chemother 63:10.1128/aac.02133-18.

604 ## List of Tables

605 **Table 1. Primers and probes used in this study**

ID	Target sequence	Sequence	Reference
oriC F1	*gidA*	CGC AAC AGC ATG GCG ATA AC	PMID: 30297723
oriC R1	*gidA*	TTC GAT CAC CCC TGC GTA CA	PMID: 30297723
ter F1	*dcp*	TCA ACG TGC GAG CGA TGA AT	PMID: 30297723
ter R1	*dcp*	TTG AGC TGC GCT TCA TCG AG	PMID: 30297723
UPEC *oriC* Probe	*gidA*	/56-FAM/ACC CAT GAT /ZEN/GTG ATC CGC AGT AAC CTC GAT CGT A/3IABkFQ/	This study
UPEC *ter*C Probe	*dcp*	/5SUN/CGC GCT AAA /ZEN/CCC GCC CTG CTG CTT AT/3IABkFQ/	This study
oriC F2	*gidA*	TCT CGT TTA TGG GCA ATG CG	This study
oriC R2	*gidA*	TGA TTT CTG TCG GCA AAG CG	This study
ter F2	*dcp*	GCG AGC GAT GAA TTA GCC TC	This study
ter R2	*dcp*	GCC TTC ATT CAA CAC CGT GT	This study

606

607

608

609 **Table 2. Specificity of *ori* and *ter* primers**

Template DNA source	$O:T^{PCR}$ (mean±SD)	Ct_{ori} (mean±SD)	Ct_{ter} (mean±SD)
E. coli	2.40±0.03	16.04±0.13	17.01±0.11
E. coli + *Citrobacter freundii*	2.44±0.07	16.08±0.12	17.07±0.08
E. coli + *Klebsiella pneumoniae*	2.61±0.16	15.94±0.09	17.03±0.04
E. coli + *Serratia marcescens*	2.57±0.04	16.00±0.03	17.08±0.01
E. coli + *Proteus mirabilis*	2.35±0.05	16.18±0.01	17.12±0.05
E. coli + *Acinetobacter baumanii*	2.57±0.02	15.89±0.16	16.96±0.14
E. coli + *Enterobacter hormaechei*	2.47±0.09	16.08±0.03	17.09±0.07
E. coli + *Morganella morganii*	2.46±0.03	16.01±0.07	17.02±0.06
E. coli + *Pseudomonas aeruginosa*	2.43±0.07	16.09±0.04	17.08±0.08
E. coli + *Bacillus subtilis*	2.41±0.03	16.09±0.12	17.07±0.14
E. coli + *Staphylococcus aureus*	2.46±0.19	15.93±0.18	16.93±0.08
Matrix control	0.98±0.06	34.53±0.03	35.95±0.37
Naive mouse kidney	ND	37.81±0.42	>40
Citrobacter freundii	ND	35.5±0.36	>40
Klebsiella pneumoniae	ND	30.24±0.07	>40
Serratia marcescens	ND	>40	>40
Proteus mirabilis	1.43±0.44	35.64±0.47	37.32±0.93
Acinetobacter baumanii	ND	37.41±0.37	>40
Enterobacter hormaechei	ND	37.2±0.55	>40
Morganella morganii	ND	36.94±0.1	>40
Pseudomonas aeruginosa	ND	>40	39.47±0.04
Bacillus subtilis	ND	>40	>40
Staphylococcus aureus	ND	>40	38.18±0.63

610 Note: ND=Not determined

611

612

613

614

615

Table 3. *E. coli* doubling time in murine urine during experimental UTI

	Doubling time (minutes) [Median (Min-Max)]	
Hours post-infection (hpi)	HM56	HM86
6	47.4 (31.6-105.2)	54.2 (31.3-90.5)
24	64.2 (28.9-153.1)	67.6 (38.3-142.5)
48	65.5 (36.8-70.9)	70.4 (46.9-89.1)
72	68.9 (59.8-148.0)	63.6 (42.0-99.7)
96	68.6 (55.3-128.1)	73.1 (64.5-76.8)
120	60.1 (46.4-70.1)	56.3 (40.8-80.5)
144	65.8 (58.5-68.4)	86.1 (52.8-104.1)
168	90.9 (63-129.1)	75.8 (46.5-139.2)

Figure legends

Fig. 1. Determination of growth rate by PTR. Stages of bacterial growth representing their ori: ter (one of the examples of *ori: ter* during exponential and stationary phase is shown. *ori,* green*; ter,* red).

Fig. 2. Validating multiplexed quantitative PCR with whole genome sequencing as a tool for measuring origin to terminus ratios in vitro. Growth experiments of *E. coli* strain HM86 in different growth medium conditions are plotted as OD_{600} reading (A) (mean ± SD). Means and standard deviation from three independent experiments are shown for TB (red), LB (black), and $M9_{Glc}$ (blue). Three biological replicates for TB, and LB, and two biological replicates for $M9_{Glc}$. (B) illustrates the example of the sequencing coverage across the genome of HM86 grown in vitro in LB up to 6h. Genomic location of origin (*ori*) and terminus (*ter*) of replication are denoted by peak and trough respectively. PTR determined by WGS is plotted in (C) (mean ± SD). (D) plots from the $O:T^{PCR}$ values (mean ± SD). Scatterplot with linear regression for the relationship between PTR derived from WGS and *ori:ter* by qPCR method in TB (E), LB (F), and $M9_{Glc}$ (G). N= 3 replicates (TB and LB), and N=1 ($M9_{Glc}$). Pearson correlation coefficient (*r*) with *p*-values are shown in the graph. Statistical significance. **** p<.0001; *p<.05). Filled symbols in the graph A, C, and D indicates the data points with active replication included in the study for growth rate determination.

Fig. 3: Bacterial growth rate correlates with $O:T^{PCR}$. Graph represents the correlation between GR and *ori:ter*-values determined by qPCR method in TB+LB+$M9_{Glc}$ (A). TB and LB=3 biological replicates, $M9_{Glc}$= 2 biological replicates. Pearson correlation coefficient (*r*) with *p*-value is shown in the graph. Statistical significance: **** p<.0001; **p<.01). Bacterial growth rate calculated from the OD_{600} reading and the $O:T^{PCR}$ in TB+LB+$M9_{Glc}$ combined is plotted in Fig. B. Statistical significance was determined using the paired *t*-test, with *p*-value<0.05 considered a significant difference.

660

661 **Fig. 4: PCR assay optimization.** Standard curves (Ct vs log_{10}CFU) (A), and (Ct vs total
662 DNA) (B) with their associated *ori:ter* determined by qPCR. Three replicates of the
663 bacterial culture at exponential phase of growth (time point 2 h) was used for DNA
664 extraction and determination of $O:T^{PCR}$ [CFU vs *ori:ter* experiment (mean ± SEM)], and
665 3 independent experiment for total DNA vs *ori:ter* (mean ± SEM). The graph depicts *E.*
666 *coli* strain HM86 *ori:ter*, Ct_{ori}, and Ct_{ter} in presence and absence of murine kidney DNA
667 (data from 3 biological replicate with 3 technical replicates) as indicated in figure
668 legends. EC (*E. coli* DNA) and mK (murine kidney DNA). DNA (data from 3 biological
669 replicates with 3 technical replicates) as indicated in figure legends. Ct (threshold cycle),
670 EC (*E. coli* DNA) and kidney (murine kidney DNA).

671

672 **Fig. 5: Bacterial burden in murine model of ascending UTI.** Experimental plan for
673 mouse model of ascending UTI (A)**.** CBAJ mice (n=5 per time point) were inoculated
674 with either HM56 or HM86 with ~$2*10^8$ CFU. Viable bacterial load in urine (B), bladder
675 (C) and kidneys (D) were determined by dilution plating in LB agar at specific time point
676 as mentioned in the plot. The horizontal dashed line indicates the limit of detection
677 (LOD). Differences between time points were assessed by the Kruskal-Wallis test.
678 Statistical significance differences are denoted by * where $p<0.05$.

679

680 **Fig. 6: $O:T^{PCR}$ in urine samples over infection period.** Box and whiskers plots, where
681 box represents the median and interquartile ranges and whiskers represents minimum
682 and maximum values for each time during infection for HM56 (A), and HM86 (B). n= 5-
683 15 mice per time point. Differences between time points were assessed by the Kruskal-
684 Wallis test. Statistical significance differences are denoted by * where $p<0.05$.

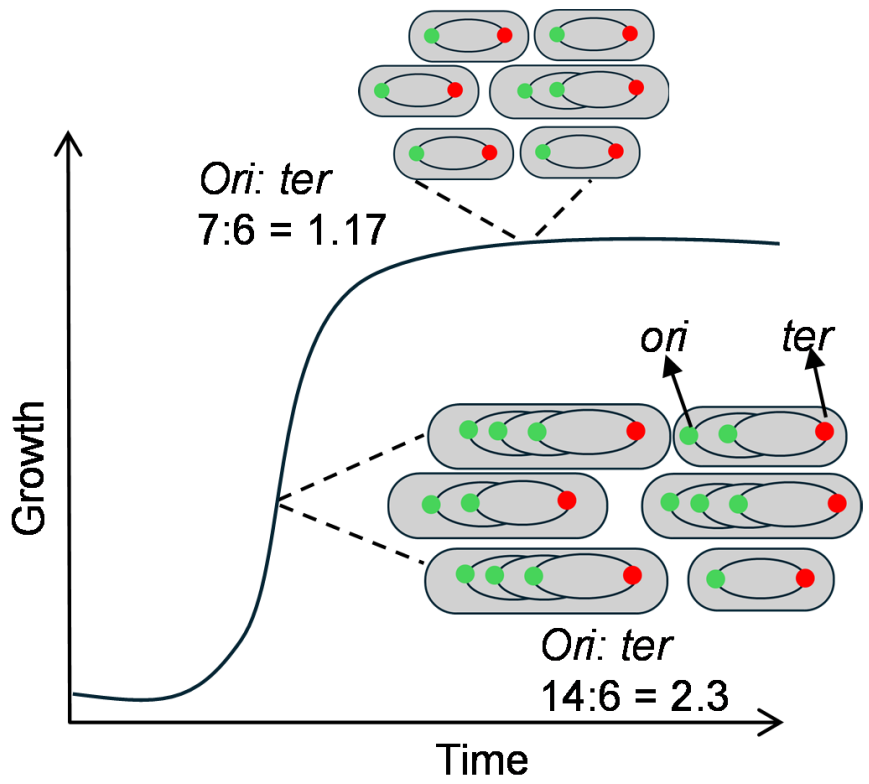

685

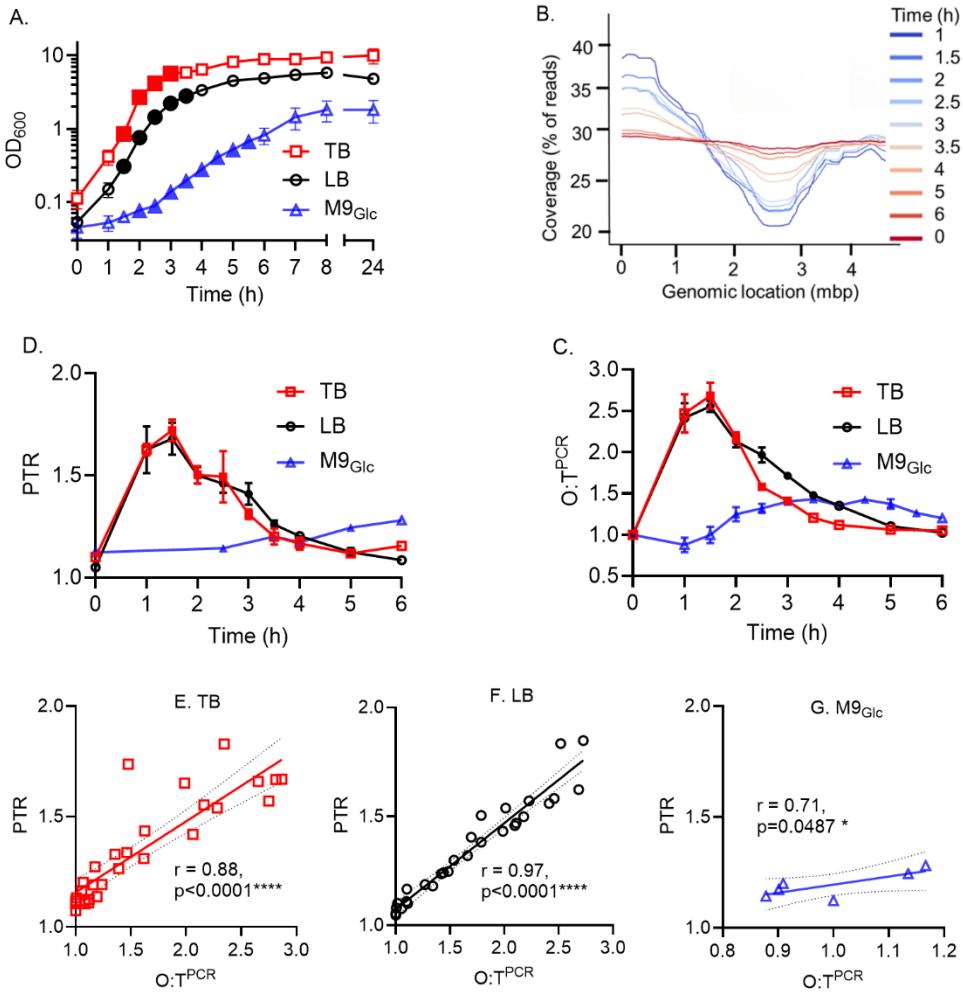
A.
OD600
Time (h)
TB
LB
M9Glc
B.
Coverage (% of reads)
Genomic location (mbp)
Time (h)
1
1.5
2
2.5
3
3.5
4
5
6
0
D.
PTR
Time (h)
TB
LB
M9Glc
C.
O:TPCR
Time (h)
TB
LB
M9Glc
E. TB
PTR
O:TPCR
r = 0.88,
p<0.0001****
F. LB
PTR
O:TPCR
r = 0.97,
p<0.0001****
G. M9Glc
PTR
O:TPCR
r = 0.71,
p=0.0487 *

686

687

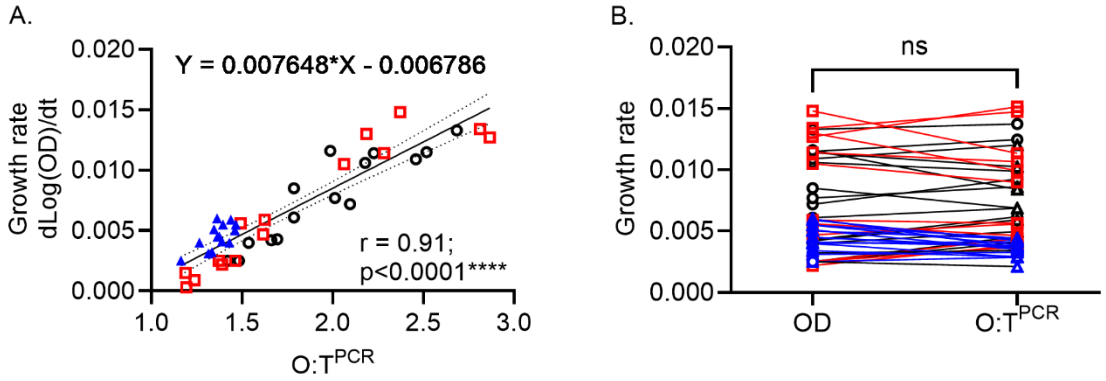
A.
Y = 0.007648*X - 0.006786
r = 0.91;
p<0.0001****
Growth rate
dLog(OD)/dt
0.020
0.015
0.010
0.005
0.000
1.0
1.5
2.0
2.5
3.0
O:T^PCR
B.
ns
Growth rate
0.020
0.015
0.010
0.005
0.000
OD
O:T^PCR

688

689

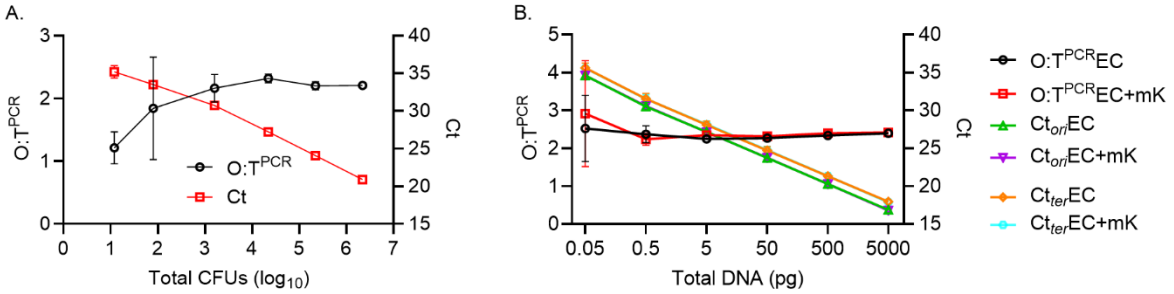
A.
O:T^PCR
Ct
O:T^PCR
Ct
Total CFUs (log10)
B.
O:T^PCR
Ct
Total DNA (pg)
O:T^PCREC
O:T^PCREC+mK
Ct_ori EC
Ct_ori EC+mK
Ct_ter EC
Ct_ter EC+mK

690

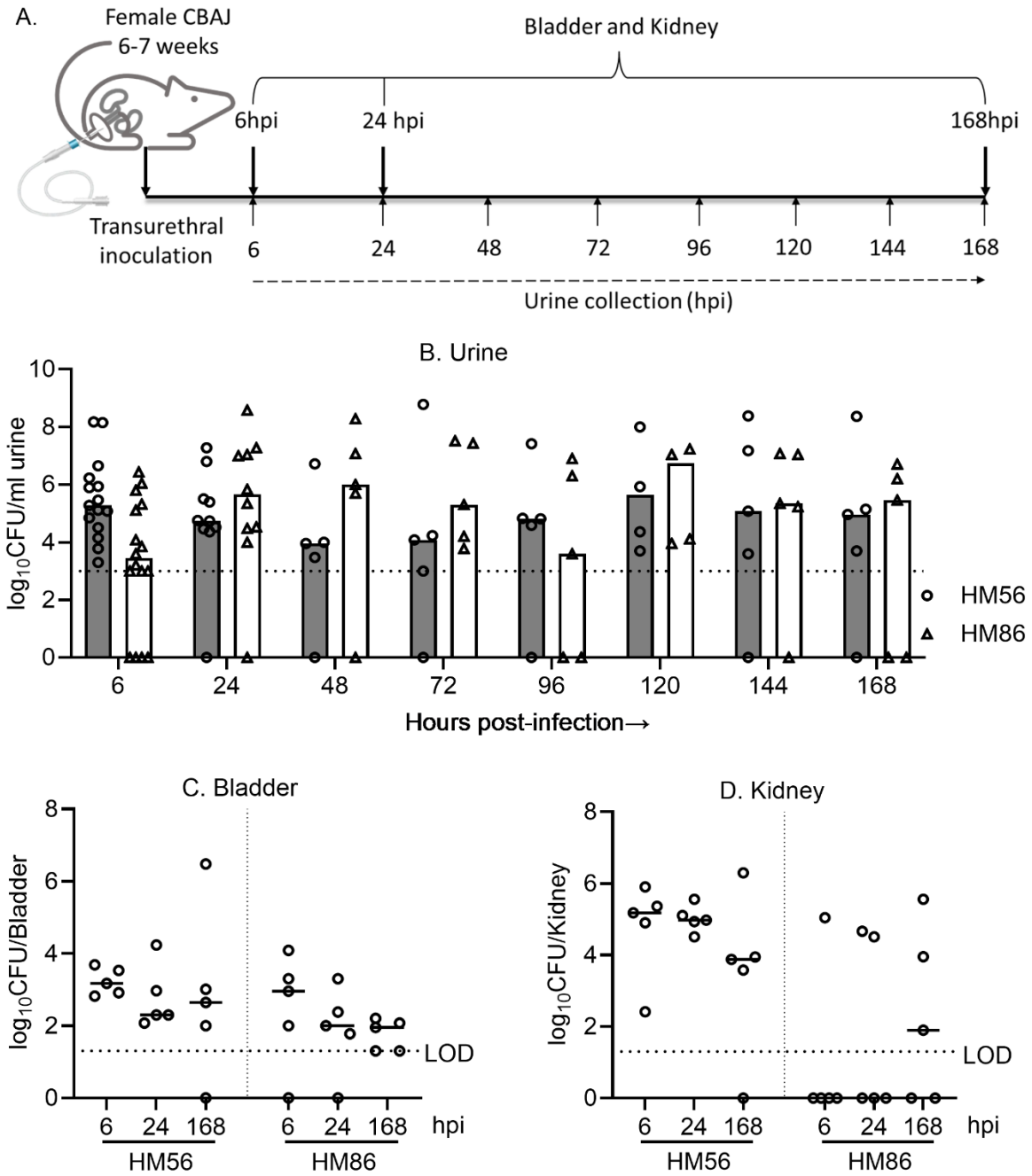
A.
Female CBAJ
6-7 weeks
Bladder and Kidney
6hpi
24 hpi
168hpi
Transurethral
inoculation
6
24
48
72
96
120
144
168
Urine collection (hpi)
B. Urine
log10CFU/ml urine
HM56
HM86
Hours post-infection→
C. Bladder
log10CFU/Bladder
LOD
hpi
HM56
HM86
D. Kidney
log10CFU/Kidney
LOD
hpi
HM56
HM86

691

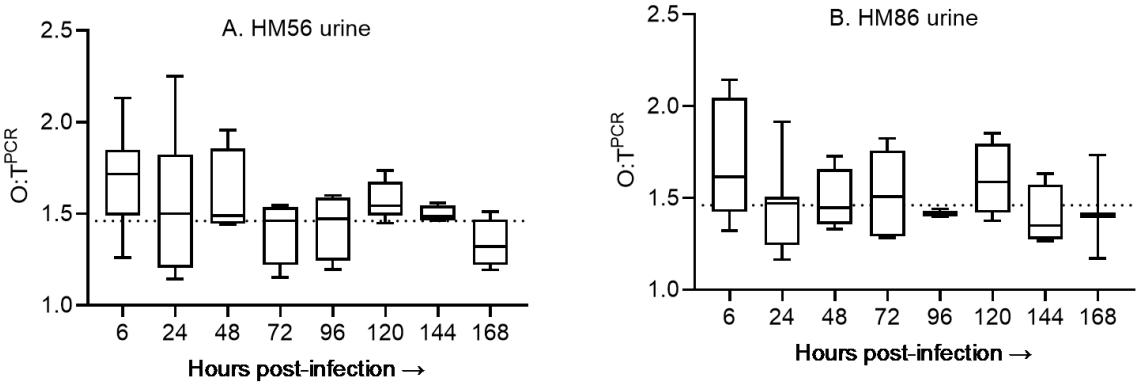
A. HM56 urine
B. HM86 urine
O:T^PCR
2.5
2.0
1.5
1.0
6
24
48
72
96
120
144
168
Hours post-infection →

692